Vortex Chirality in Exchange-Biased Elliptical Magnetic Rings

W. Jung, F. J. Castaño, and C. A. Ross*

Department of Materials Science and Engineering, Massachusetts Institute of Technology, Cambridge, Massachusetts 02139, USA

(Received 20 June 2006; published 15 December 2006)

The flux-closed or ''vortex'' state in thin-film magnetic rings has been proposed as a data storage token, but it has proven difficult to control the vortex chirality in a simple manner. Here, a model is described that predicts the vortex chirality of an elliptical magnetic ring as a function of the direction of the applied field and of the exchange bias, based on the change in energy of the system as the domain walls move. Experimental measurements of chirality in Co and Co/IrMn magnetic rings with 3.2 μm major axis are in excellent agreement with the model. The vortex circulation direction can therefore be tailored with an appropriate combination of applied field direction and exchange bias direction with respect to the major axis.

DOI: 10.1103/PhysRevLett.97.247209 PACS numbers: 75.70.Cn, 75.30.Gw, 75.60.Ch, 85.70.Kh

Magnetization reversal and equilibrium magnetic states of thin-film ferromagnetic disks and rings have been extensively studied in recent years [1–5]. Several topologically distinct magnetic states have been observed in disks and rings, but particular attention has been given to the flux-closed or ''vortex'' state, in which the magnetization is oriented circumferentially and there are no domain walls. This state has been proposed for data storage devices in which the chirality of the magnetization rotation is utilized to store a data bit [6], as was practiced in one of the first-generation computer memories, the magnetic core memory. Much work has been devoted to the investigation of the chirality of the vortex in rings and disks under the influence of an in-plane magnetic field, because control of the rotation sense is essential for applications, for example, in data storage and sensors. The chirality has been manipulated by introducing notches or a flat edge to rings [7–9] and disks [10,11], and rings with an off-centered core [12–14] exhibit a preference for one circulation direction. However, there has been little work on the control of chirality in circular rings other than by introducing geometrical asymmetries, and vortex control in elliptical rings has not been analyzed.

As a tunable source of unidirectional anisotropy, exchange bias can be introduced to thin-film disks and rings by employing a ferromagnetic (FM)/antiferromagnetic (AFM) bilayer structure [15]. The exchange bias can affect the formation and chirality of the vortex state. For example, in NiFe/IrMn disks a vortex forms during reversal only when the applied field orientation is close to the exchange pinning direction [16,17], and circumferential exchange bias in rings with a flat edge has been used to control the vortex chirality [18]. In this Letter, we model the vortex formation in single-layer and exchange-biased elliptical rings analytically, by considering the energy change resulting from the motion of the domain walls when a ring is reversed from the bidomain or ''onion'' state attained after saturation (a state with two 180° domain walls, one at each end of a diameter). We demonstrate how the vortex chirality can be controlled by the directions of the applied field and the exchange bias with respect to the major axis of the ring.

Arrays of elliptical rings with a major diameter of 3.2 μm, minor diameter of 2 μm and widths of 400–500 nm were fabricated using electron-beam lithography and lift-off processing. Single-layer rings were made from polycrystalline Co (12 nm) films and exchange-biased rings from Co(12 nm)/IrMn(5 nm) bilayer structures, with a Ta (10–20 nm) seed layer and Cu (2 nm) capping layer. Co films were deposited by ion beam sputtering at an Ar pressure of 3.5×10^{-5} Torr, a beam current of 35 mA and a beam voltage of 1000 V. The other materials were grown by dc triode magnetron sputtering at a pressure of 1 mTorr Ar. The base pressure of the sputter chamber was below 9×10^{-9} Torr. An *in situ* magnetic field of 350 Oe was applied during the growth of exchange bias structures in order to induce a bias on the FM layer parallel to the field direction. The exchange bias of unpatterned Co/IrMn films was 75 Oe. The magnetic states of the rings were imaged at remanence using a Digital Instruments Nanoscope magnetic force microscope (MFM) with a low moment tip at a scan height of 30 nm. Figure 1 shows two rows of Co rings, where each ring has a different major axis direction. Each sample consisted of 13 such rows. In the Co/IrMn sample the exchange bias direction is parallel to the rows of ellipses.

In ferromagnetic rings, switching from the onion state to the vortex state typically takes place as one of the domain walls of the onion state unpins and moves until it ap-

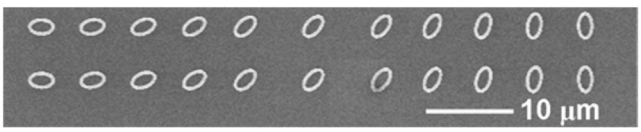

FIG. 1. Scanning electron micrograph of two rows of Co elliptical rings with major diameter 3.2 μm, minor diameter 2 μm, and width 400 nm.

proaches and annihilates the other wall [2]. A field applied opposite to the saturation direction initiates the movement of the domain walls and they are expected to move such that the Zeeman energy of the system is reduced. The chirality of the resulting vortex state depends on the direction of motion of whichever wall moves first. In the case of symmetric rings, the Zeeman energy reduction is not influenced by the direction [clockwise (CW) or counterclockwise (CCW)] of domain wall motion. The preference for a particular direction of wall motion typically emerges when a ring shows asymmetry in its shape [7,9,12,14]. In the case of an elliptical ring, the curvature varies around the ring, and one may expect a preference for the direction of wall motion if the field is applied at an angle away from the major or minor axes. To model this response, the change in Zeeman energy was calculated for CW and CCW motion of a domain wall. If α represents the angle between the applied field $\mathbf{H_a}$ and the major axis, θ the angle through which the wall has rotated around the ring, $\mathbf{M}_s$ the saturation magnetization, and V the volume of the segment where magnetization has been reversed (Fig. 2) then the energy change is given by

$$2\int_V \vec{M}_s \cdot \vec{H}_a dV.$$

This expression was evaluated numerically for a range of values of α for the geometry of the Co ring samples. The ring was discretized into 100 circumferential strips, each of which was divided into 360 cells. The integral above was evaluated as the sum of inner products of $\mathbf{M_s}$ and $\mathbf{H_a}$ for each cell, multiplied by the volume of the cell, for the region of the ring that reversed (i.e., for a wall moving through angle θ). The magnetization $\mathbf{M_s}$ is assumed to be always parallel to the edges of the ring but it changes in direction by 180° as a result of wall motion. The magnitude of $\mathbf{H_a}$ was set at 150 Oe, corresponding to the average onion-to-vortex switching field obtained from the MFM measurements. The ring is assumed to have been previously saturated by a field opposite to $\mathbf{H_a}$, and this determines the position of the walls at remanence, prior to application of $\mathbf{H_a}$. The initial domain wall positions were determined experimentally from the MFM images of the remanent onion state of Co elliptical rings measured here [Fig. 3(i)]. They were in general not coincident with the applied field direction, but were displaced towards the major axis of the ellipse. For example, at $\alpha = 0°$, 30°, 60°, and 90° the remanent wall positions are at 0°, 11°, 32°, and 90°, respectively, to the major axis.

Figure 2 shows the change in Zeeman energy calculated for several field angles α as one of the domain walls rotates by $\alpha \leq \pm 90°$. As expected, for a field applied along the major axis ($\alpha = 0°$) or minor axis ($\alpha = 90°$), the result is symmetric for CW and CCW wall motion, but at other angles, the curves become asymmetric. The direction of domain wall rotation can be inferred from the slope of the curve of energy vs θ at $\theta = 0°$. The walls of the onion state are predicted to rotate counterclockwise if the field is

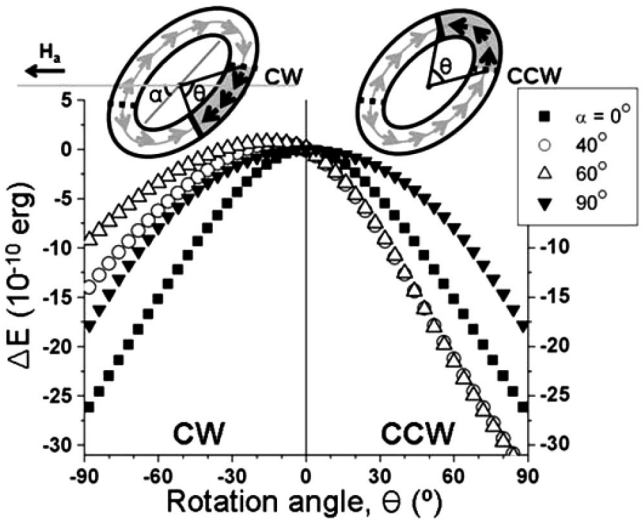

FIG. 2. Top: schematic diagram describing the motion of domain walls of the onion state in a field H_a applied at angle α to the major axis. The ring was previously saturated opposite to the field direction. The dotted lines represent the initial domain wall positions, and the solid lines the final wall position after one of the walls has rotated by θ. The gray arrows correspond to the original magnetization direction of the onion state and the reversed magnetization region is represented by black arrows. Bottom: Zeeman energy change as a function of the domain wall rotation angle θ for different applied field angles α, after saturation opposite to the field direction. The calculation was carried out for rings with the same geometry as in Fig. 1.

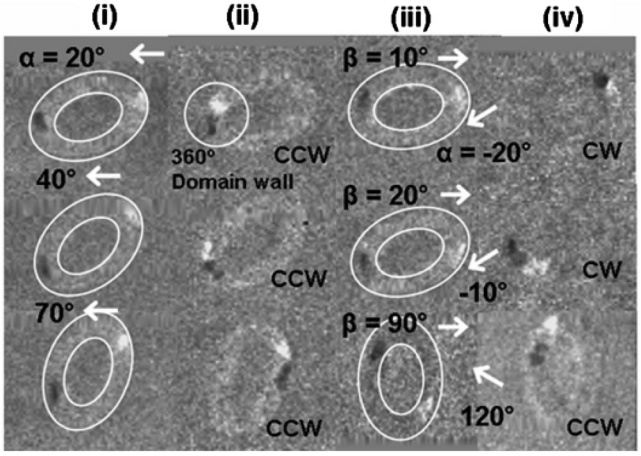

FIG. 3. MFM images of Co (i),(ii) and Co/IrMn (iii),(iv) elliptical rings after saturation (i), (iii) and after applying a reverse field of 232 Oe (ii), and 200 Oe (iv) at an angle α. The rings in columns (iii) and (iv) are exchange biased at angle β. Rings (i) and (iii) are outlined for clarity. In (ii) the contrast of a 360 ° wall is shown with an outline. Each image of a twisted state in columns (ii) and (iv) is labeled with a letter showing the wall motion direction that generated it.

oriented between $\alpha = 0°$ and 90°, and clockwise if the field is oriented between $\alpha = -90°$ and 0°.

Experimental confirmation of these results was accomplished by observation of the domain walls in the rings by MFM. MFM cannot measure vortex chirality directly because of the lack of stray fields in the vortex state, but the chirality can be inferred by observing the contrast of the ''twisted'' magnetic state that precedes vortex formation [19,20]. The twisted state is a metastable magnetic state which is formed during the onion-to-vortex transition by the movement of one of the onion state 180° domain walls towards the other to form an in-plane 360° wall. This structure can exist over an extensive field range, and at remanence, but is ultimately annihilated to generate the vortex state. The contrast of the twisted states in the MFM images enables determination of which domain wall moved first, and whether it moved CW or CCW.

Figure 3 shows the contrast of several twisted states in rings measured at different values of α. The sample contains 143 rings in total, with 11 different major axis directions. For a given reverse field near the onion-to-vortex transition, about 5% of the rings exhibit twisted states. Several twisted states were found for each value of α. The twisted states consistently demonstrated CCW rotation of the domain walls for all field angles between $\alpha = 0°$ and 90°, in agreement with the calculation results. For example, in Fig. 3(ii), in the sample with $\alpha = 20°$ the bright-contrast domain wall rotated CCW along the upper arm of the ring, whereas in the sample with $\alpha = 70°$ the dark-contrast domain wall also moved CCW but traveled along the lower arm of the ring. These results show that in elliptical rings the desired chirality of the vortex state can be obtained by switching the rings from the onion state using an appropriate field direction, and are analogous to vortex control by unpinning of walls in notched rings [8].

Vortex chirality in exchange bias elliptical rings presents a more complex situation because the angle β between the exchange bias direction and the major axis also influences the wall motion. The model was modified to include exchange bias by adding the inner product of the exchange field and the magnetization to the energy term, so that changes in both Zeeman and exchange energy could be calculated as a domain wall rotates either clockwise or counterclockwise. The exchange field of the rings was taken to be the same as that of the unpatterned film, as found previously [21]. Initial domain wall positions of the rings were measured systematically from MFM images such as those in Fig. 3(iii), for a range of α and β.

Figure 4 shows the energy for a ring with $\beta = 60°$, for field angles of $\alpha = 0$, 30°, 60°, and 90°. In contrast to the unbiased ring, the change in energy vs wall displacement angle $\Delta E(\theta)$ for $\alpha = 0°$ is no longer symmetrical, and indicates a preference for CW wall motion. For $\alpha = 30°$ the motion is CW, but for $\alpha = 90°$ the motion is CCW. The critical field angle α_c at which the wall motion changes

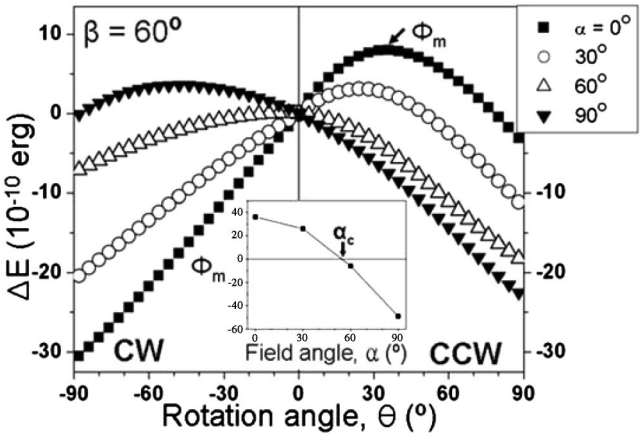

FIG. 4. The calculated energy change in a 500 nm wide exchange-biased elliptical ring for different field angles α as a domain wall rotates clockwise or counterclockwise through angle θ. The exchange pinning angle β was 60°. The value of $\theta = \Phi_m$ at which each curve has a maximum is plotted vs field angle α in the inset. This passes through zero at $\alpha_c = 55°$ for this particular ring geometry and exchange bias direction.

sign corresponds to the value of α at which $\Delta E(\theta)$ has a maximum at $\theta = 0°$, which in this case is approximately 55° (inset of Fig. 4). For this particular ring geometry and material the critical field direction α_c is close to the exchange bias direction β because the exchange anisotropy is large compared with the shape anisotropy of the elliptical ring. For circular rings, we expect $\alpha_c = \beta$, while for elliptical rings, as the shape anisotropy increases compared to the exchange anisotropy, α_c will approach zero (coincident with the major axis of the ring).

Based on a series of calculations for various values of α and β, a phase diagram of CW and CCW domain wall rotation, i.e., a phase diagram of the vortex chirality, was plotted (Fig. 5). The boundary between the two regimes, at α_c, is located near the line $\alpha = \beta$. This phase diagram was compared with the MFM images of the twisted states in the exchange-biased elliptical rings. Examples of MFM data are given in Fig. 3(iv), which shows CW wall motion for $\alpha = -20°$, $\beta = 10°$, and for $\alpha = -10°$, $\beta = 20°$, and CCW motion for $\alpha = 120°$, $\beta = 90°$.

The points where one or more twisted states were found were marked on the phase diagram with different symbols depending on the direction of domain wall rotation. These experimental data points are almost entirely in agreement with the findings from the calculation, and support the model that predicts the CW or CCW direction of movement of the domain walls. Rings with $\alpha \approx \alpha_c$ show CW or CCW wall motion approximately equally. As in the single-layer Co rings, there was no preference for which of the two domain walls in the onion state moved first, only for the direction of movement.

This work demonstrates that the direction of vortex circulation in exchange-biased elliptical rings can be con-

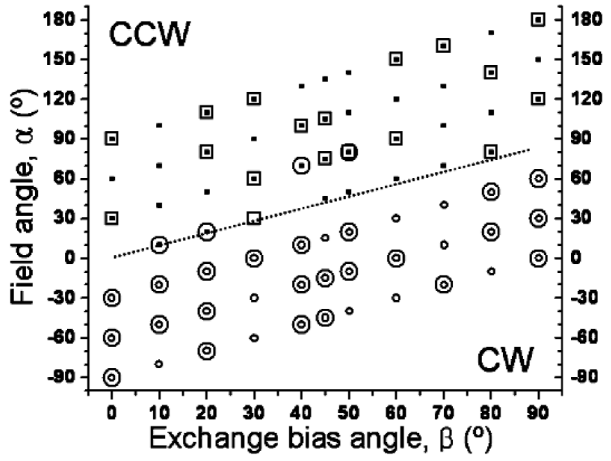

FIG. 5. Phase diagram of the vortex chirality of a 500 nm wide exchange-biased elliptical ring as a function of the external field angle α and exchange bias angle β. The small solid squares represent the points where counterclockwise circulation is predicted by the calculation and small open circles represent clockwise circulation. The critical field angle, $\alpha_c(\beta)$, is shown by a dotted line close to $\alpha = \beta$, along which there is no preference for either wall motion direction. The large open squares and circles indicate experimental observations of the chirality of the twisted state, the precursor to the vortex state: squares for CCW chirality and circles for CW chirality.

trolled by modifying the field and exchange bias angles. Moreover, the fact that exchange-biased elliptical rings respond differently to the same reverse field compared with single-layer rings is noteworthy. For example, using the geometry and layer thicknesses in this experiment, if a reverse field at $\alpha = 30°$ is applied to an exchange-biased elliptical ring pinned at $\beta = 60°$, the domain wall in the ring would rotate clockwise, while the domain wall in a single-layer Co ring would rotate counterclockwise in the same field, leading to antiparallel vortices. This characteristic suggests that in a structure comprised of a multilayer stack containing both pinned and unpinned rings, for example, a spin valve, a desired vortex state can be obtained independently in each ferromagnetic layer by using the effects of shape and exchange bias. Also the tunability of the exchange bias direction by field cooling can be used for postproduction control of the vortex chirality, which is unavailable from shape anisotropy. This modeling approach can be generalized to other geometries and materials, and will be valuable in understanding the behavior of ring-shaped magnetoelectronic or sensor devices.

The authors acknowledge the financial support of the National Science Foundation and the Cambridge-MIT Institute.

*Corresponding author.
Electronic address: caross@mit.edu

[1] C. A. Ross, F. J. Castano, D. Morecroft, W. Jung, H. I. Smith, T. A. Moore, T. J. Hayward, J. A. C. Bland, T. J. Bromwich, and A. K. Petford-Long, J. Appl. Phys. **99**, 08S501 (2006).
[2] J. Rothman, M. Klaui, L. Lopez-Diaz, C. A. F. Vaz, A. Bleloch, J. A. C. Bland, Z. Cui, and R. Speaks, Phys. Rev. Lett. **86**, 1098 (2001).
[3] T. Shinjo, T. Okuno, R. Hassdorf, K. Shigeto, and T. Ono, Science **289**, 930 (2000).
[4] R. P. Cowburn and M. E. Welland, Science **287**, 1466 (2000).
[5] R. P. Cowburn, D. K. Koltsov, A. O. Adeyeye, M. E. Welland, and D. M. Tricker, Phys. Rev. Lett. **83**, 1042 (1999).
[6] J. G. Zhu, Y. F. Zheng, and G. A. Prinz, J. Appl. Phys. **87**, 6668 (2000).
[7] M. Klaui, J. Rothman, L. Lopez-Diaz, C. A. F. Vaz, J. A. C. Bland, and Z. Cui, Appl. Phys. Lett. **78**, 3268 (2001).
[8] M. Klaui, C. A. F. Vaz, J. A. C. Bland, W. Wernsdorfer, G. Faini, and E. Cambril, Appl. Phys. Lett. **81**, 108 (2002).
[9] R. Nakatani, T. Yoshida, Y. Endo, Y. Kawamura, M. Yamamoto, T. Takenaga, S. Aya, T. Kuroiwa, S. Beysen, and H. Kobayashi, J. Appl. Phys. **95**, 6714 (2004).
[10] T. Taniuchi, M. Oshima, H. Akinaga, and K. Ono, J. Appl. Phys. **97**, 10J904 (2005).
[11] M. Schneider, H. Hoffmann, and J. Zweck, Appl. Phys. Lett. **79**, 3113 (2001).
[12] P. Vavassori, R. Bovolenta, V. Metlushko, and B. Ilic, J. Appl. Phys. **99**, 053902 (2006).
[13] F. Q. Zhu, G. W. Chern, O. Tchernyshyov, X. C. Zhu, J. G. Zhu, and C. L. Chien, Phys. Rev. Lett. **96**, 027205 (2006).
[14] E. Saitoh, M. Kawabata, K. Harii, H. Miyajima, and T. Yamaoka, J. Appl. Phys. **95**, 1986 (2004).
[15] J. Nogues, J. Sort, V. Langlais, V. Skumryev, S. Surinach, J. S. Munoz, and M. D. Baro, Phys. Rep.- Rev. Sec. Phys. Lett. **422**, 65 (2005).
[16] J. Sort, G. Salazar-Alvarez, M. D. Baro, B. Dieny, A. Hoffmann, V. Novosad, and J. Nogues, Appl. Phys. Lett. **88**, 042502 (2006).
[17] J. Sort, A. Hoffmann, S. H. Chung, K. S. Buchanan, M. Grimsditch, M. D. Baro, B. Dieny, and J. Nogues, Phys. Rev. Lett. **95**, 067201 (2005).
[18] R. Nakatani, T. Yoshida, Y. Endo, Y. Kawamura, M. Yamamoto, T. Takenaga, S. Aya, T. Kuroiwa, S. Beysen, and H. Kobayashi, J. Magn. Magn. Mater. **286**, 31 (2005).
[19] F. J. Castano, C. A. Ross, A. Eilez, W. Jung, and C. Frandsen, Phys. Rev. B **69**, 144421 (2004).
[20] F. J. Castano, C. A. Ross, and A. Eilez, J. Phys. D **36**, 2031 (2003).
[21] W. Jung F. J. Castano, D. Morecroft, C. A. Ross, R. Menon, and H. I. Smith, J. Appl. Phys. **97**, 10K113 (2005).